journal

J. Am. Ceram. Soc., 84 [3] 551–54 (2001)

Cyclic Fatigue–Crack Propagation Behavior in Silicon Carbide: Long- and Small-Crack Behavior

Yoon Soo Han and Do Kyung Kim*

Department of Materials Science and Engineering, Korea Advanced Institute of Science and Technology, 373-1 Kusung-Dong, Yusong-Gu, Taejon, 305-701, Korea

Christopher J. Gilbert* and Robert O. Ritchie

Materials Sciences Division, Lawrence Berkeley National Laboratory, and Department of Materials Science and Mineral Engineering, University of California, Berkeley, California 94720

Cyclic fatigue properties of high-toughness SiC with additives of Al_2O_3 and Y_2O_3 were examined, with a focus on differences between long- (>3 mm) and small-crack (<200 μm) behavior. Small cracks were initiated with Vickers indents placed on the tensile surfaces of beams, and crack extension was monitored optically under cyclic load. For small cracks, high growth rates which exhibited a negative dependence on the far-field driving force were observed. Such behavior was explained by both indent-induced residual stresses and the relative size of cracks compared with bridging zone lengths.

I. Introduction

In the past decade, one of the problems in liquid-phase-sintered (LPS) silicon carbide, despite excellent high-temperature properties, is that the fracture toughness is relatively low (~2–3 MPa·$m^{1/2}$ at room temperature).[1] However, silicon carbide with a fracture toughness above 7 MPa·$m^{1/2}$ was reported recently in the case of SiC sintered with an oxide liquid phase; for silicon carbide sintered with aluminum, boron, and carbon, fracture toughness of above 9 MPa·$m^{1/2}$ was achieved.[2–7] It is believed that platelike grains were formed during heat treatment (due to the α-to-β phase transformation), and that these (like rocks in concrete) play an important role in crack bridging.[8–11]

Despite the fracture toughness increase, it is known that crack resistance in the long-crack region (>~3 mm) is different from that in the small-crack region (<~250 μm) in many *in situ* toughened ceramics showing a rising resistance curve. It is well explained that decreasing crack resistance in the small-crack region results from an undeveloped crack wake zone at the crack tip. There are few reports showing the relationship between fatigue crack growth rates and driving force in small- and long-crack regions.[12,13] Therefore, life prediction methods based on long-crack measurements may be nonconservative. Moreover, it is pointed out that small-crack growth behavior depends inversely on the far-field applied driving force below the threshold stress intensity (K_{th}). In these cases, the anomalous small-crack growth rate is due to the limitation of crack tip shielding and to indent-induced residual stress fields.

The present study is focused on the resistance curve, long- and small-crack growth properties in silicon carbide with an oxide liquid phase. Effects of initial crack size on crack growth rates were investigated in particular.

II. Experimental Procedure

(1) Material Processing

Starting powders were prepared by mixing β-SiC (0.3 μm diameter) and oxide powders (6 wt% Al_2O_3 + 4 wt% Y_2O_3) for liquid formation at the sintering temperature. Partially transformed SiC powder was also added (1 wt%) as seed particles to promote anisotropic grain growth. The method for preparation of seed particles was described in detail elsewhere.[14] Powders were milled in ethanol with high-purity alumina balls in a polyethylene bottle. Dried powders were capsulated in graphite foil within a graphite sleeve and hot-pressed at 1950°C for 3 h under 25 MPa and an Ar atmosphere. Sintered bodies had densities above 99%, and were disk-shaped with a 20 mm diameter and 3 mm thickness. To control grain growth, specimens were placed in a powder bed of the same composition in a graphite crucible, and heat-treated at 1950°C for 3 h under Ar atmosphere.

(2) Resistance Curve Measurement

Resistance curves for small cracks were measured via the indentation-strength method developed by Braun *et al.*[15] as follows. It was conducted on 4-point bend specimens (with nominal dimensions 3 mm × 3 mm × 20 mm with outer spans of 12.7 mm and inner spans of 6.4 mm) at 0.06 mm/min crosshead speed. Before testing, the tensile surface was polished with 1 μm diamond paste. Indentation cracks were formed under loads ranging from 5 to 100 N using Vickers indents. Each beam was examined after failure in the SEM to determine whether fracture originated from the indent cracks. After five tests at each load, data points were used to get the average value of the fracture strength. Under the action of an applied stress σ_A, radial cracks of size c, produced at the indentation load P, extend according to the equilibrium condition

$$K'_A(c) = \psi\sigma_A c^{1/2} + \chi P/c^{3/2} = T(c) \quad (1)$$

where K'_A is an effective applied stress-intensity factor, ψ is a geometrical coefficient that characterizes the pennylike crack configuration, χ is a coefficient that characterizes the intensity of the residual field in terms of indentation hardness and Young's modulus, and $T(c)$ defines the T-curve for the material. For a given indent load, P, failure is assumed to occur at the stress where the applied stress, σ_A, is equal to the fracture stress, σ_F, which satisfies the "tangency condition"

$$dK'_A(c)/dc = dT(c)/dc \quad (2)$$

N. P. Padture—contributing editor

Manuscript No. 188609. Received April 24, 2000; approved October 23, 2000.

Supported by the Korea Science and Engineering Foundation (Grant No. KOSEF 975-0800-008-2) and the U.S. National Science Foundation through the Division of International Programs (Grant No. NSF-INT-95076S3).

*Member, American Ceramic Society.

Accordingly, given an appropriate calibration of the coefficients ψ (=0.93) and χ (=0.084),[11] we may generate families of $K_A'(c)$ curves from the $\sigma_F(P)$ data sets. Toughness curves $T(c)$ may then be determined as the envelope of these families of curves.

(3) Long-Crack Growth Rates

To observe long-crack growth, half-chevron-shaped starter notches of ~3 mm were made in the disk-shaped compact-tension (DC(T)) specimens (width W = 20 mm, thickness t = 2.5 mm) after polishing one side with 1 μm diamond paste. Before data collection, samples were precracked under cyclic loading for several millimeters beyond this notch. Specimens were cyclically loaded at a load ratio (ratio of minimum to maximum stress intensity, K_{min}/K_{max}) of R = 0.1 and 0.5 and a frequency of 25 Hz (sine wave) on a high-resolution, computer-controlled servo-hydraulic test machine, operating under closed-loop displacement, load, or stress-intensity control (generally following ASTM Standard E647). To measure crack growth rates, the applied stress intensity, ΔK ($=K_{max} - K_{min}$), was controlled over a range of growth rates and fixed load ratios. Here the threshold stress was defined as stress when the maximum crack growth ratio is $<10^{-10}$ m/cycle. These techniques have been described extensively elsewhere.[11–13]

Crack size was determined using the compliance approach by a 350 Ω strain gauge attached to the back-face of the specimen. A high-resolution traveling optical microscopy (Questar QM 100, New Hope, PA) was used to confirm crack lengths, and the difference between optical and compliance readings was within 2%. From such data, crack growth rate, da/dN, as a function of both the maximum applied stress intensity, K_{max} or ΔK ($=K_{max} - K_{min}$), was plotted.

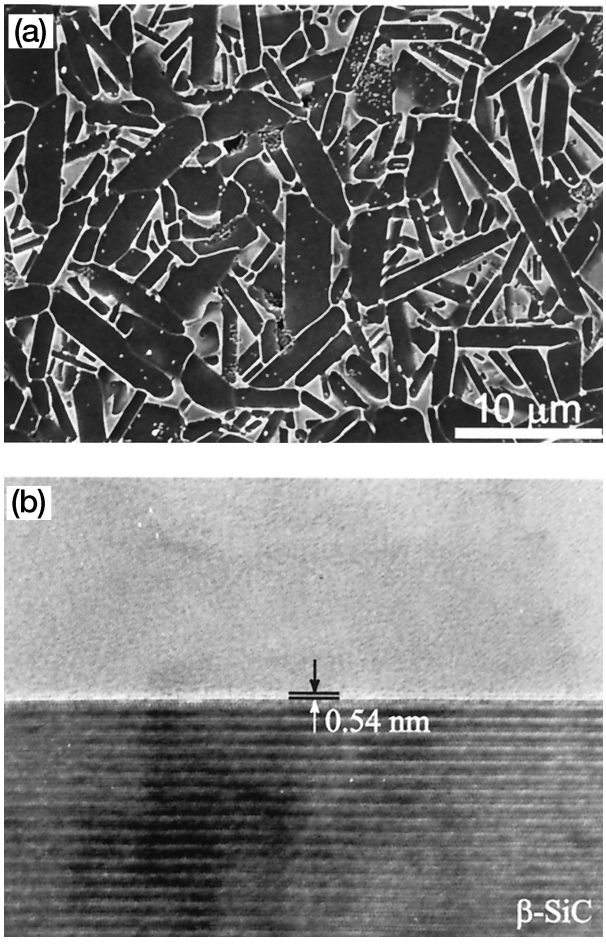

Fig. 1. (a) Scanning electron micrograph of liquid-phase-sintered silicon carbide with alumina and yttria after plasma etching. (b) High-resolution transmission electron micrograph of the interface with the liquid film. Note that the thickness of the liquid film around the elongated grain is ~0.5–0.8 nm.

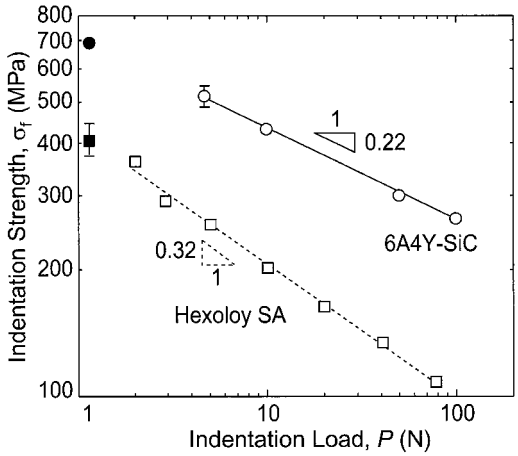

Fig. 2. Postindentation fracture strength for both the Hexoloy SA and 6A4Y-SiC is plotted as a function of indentation load. While the 6A4Y-SiC exhibits enhanced flaw tolerance, the Hexoloy SA follows a $\sigma_{m\ P}^{-1/3}$ response, indicative of single-valued toughness. The filled data point represents the nonindented strength.

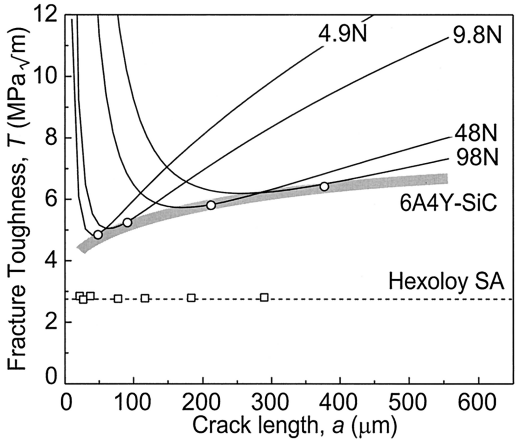

Fig. 3. Constructed R-curves from the data in Fig. 2 for both 6A4Y-SiC and Hexoloy SA (dotted line). The solid curves are plots of the total stress intensities, K_{tot}, versus crack size.

(4) Small-Crack Growth Rate

Small-crack growth rates were measured by observing small indent-initiated surface cracks on the polished tensile surfaces of cantilever beams. Sets of indents were made along the long axis, on the polished side, under the same indent load. The distance between the centers of the indents was 2 mm to avoid interference between residual stress fields. Cyclic loading was applied to a surface crack of ~100 μm initial length, until the specimen was broken or the crack no longer grew. Loading conditions were the same as long-crack tests (25 Hz sine wave, R = 0.1). For monitoring crack growth under cyclic loading, we periodically paused the machine and measured crack length via optical microscopy (×500). On achieving crack growth under constant stress, crack size was measured every 10^2 to 10^4 cycles.

The stress intensity factor, K_{max}, due to bending stresses, σ_A, was calculated from the linear elastic solution for three-dimensional surface cracks.[16] Crack growth rates were deconvoluted from the a ($=2c$) vs N (number of cycles) data for the indentation cracks, and the measured range of crack growth rates was 10^{-6} to 10^{-11} m/cycle. Cyclic crack growth rates for surface cracks were plotted as a function of the maximum stress intensity factor, K_{max}. Contributions to the driving force from indent-induced residual stress, K_{rd}, were calculated from

$$K_{rd} = \chi \frac{P}{c^{3/2}} \quad (3)$$

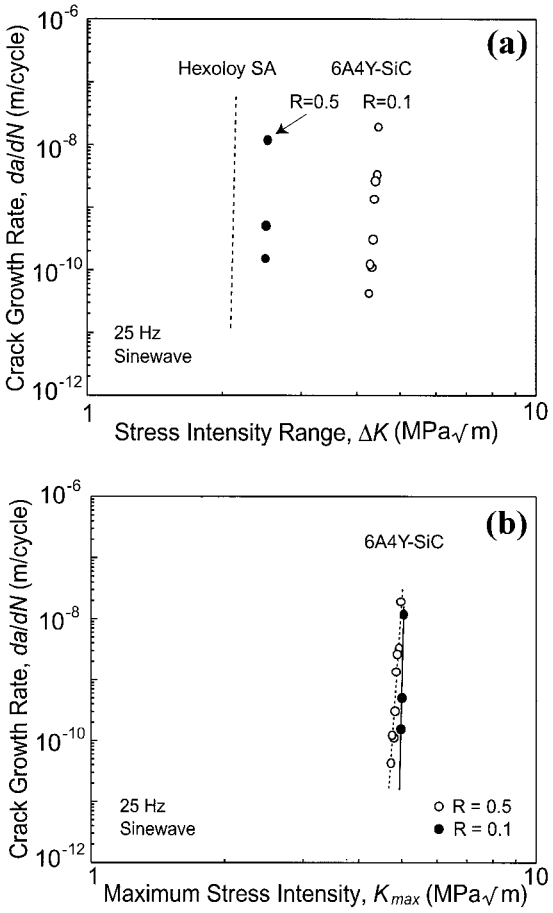

Fig. 4. (a) Influence of load ratio, *R*, on cyclic fatigue-crack growth rates, d*a*/d*N*, as measured for long (>3 mm) cracks in the 6A4Y-SiC. In (a) d*a*/d*N* is characterized in terms of the applied stress-intensity range, Δ*K*, and in (b), in terms of the maximum applied stress intensity of the loading cycle, K_{max}.

where *P* is indentation load, *c* the half-length of the surface crack size, and χ (=0.084) the coefficient of residual contact.[11] Therefore, the total stress intensity at maximum load during cyclic fatigue was

$$K_{total} = K_{max} + K_{rd} \quad (4)$$

III. Results and Discussion

(1) Microstructure

The microstructure of 6A4Y-SiC is shown in Fig. 1(a) and consists of elongated grains (longitudinal axis of 4.4 (±1.93) μm and transverse axis of 1.3 (±0.67) μm). Such elongated grains, together with the low boundary strength and compressive stresses due to the difference of thermal expansion coefficients, are believed to be the primary reason for the increase in fracture toughness through the promotion of grain bridging. High-resolution TEM studies, shown in Fig. 1(b), revealed that the thickness of the amorphous grain boundary film varied from 0.5 to 0.8 nm depending on the boundary orientation, consistent with previous results in other ceramic systems.[17–19] The fact that the boundaries appear atomically flat is an indication that they can easily slide over each other during the pullout process, which is critical in the development of rising *R*-curve behavior.

(2) R-Curve Behavior

Plots of the indentation fracture strength, σ_f, as a function of indentation load, *P*, are shown in Fig. 2 for 6A4Y-SiC (liquid-phase-sintered SiC with 6 wt% Al_2O_3 and 4 wt% Y_2O_3) and Hexoloy SA (Carborundum, Niagara Falls, NY). The data for the latter material follow a typical $\sigma_f \propto P^{-1/3}$ response, indicating a single-valued toughness or flat *R*-curve. By comparison, the degradation in strength with indentation load for 6A4Y-SiC is much shallower, indicating a more pronounced flaw tolerance with higher strength retention even with large flaw sizes. The data in Fig. 2, along with the above calibrated values for χ and ψ, are used to deconvolute a small-crack *R*-curve for both the 6A4Y-SiC and the Hexoloy SA (Fig. 3), following the indentation-strength *K*-field analysis of Braun *et al.* described above.[15]

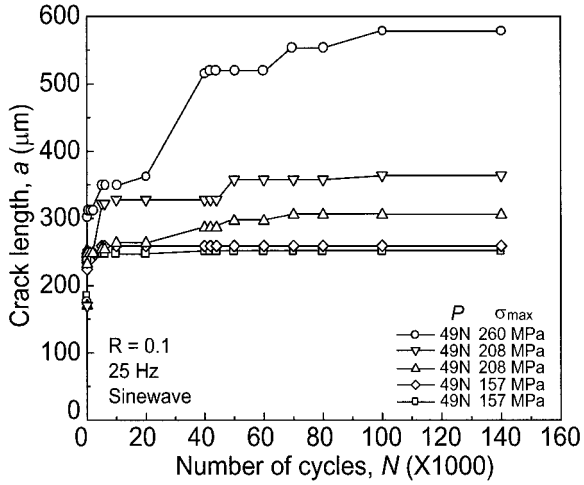

Fig. 5. Small-crack data in 6A4Y-SiC showing the variation in surface crack length, 2*c*, with number of cycles at $R = 0.1$.

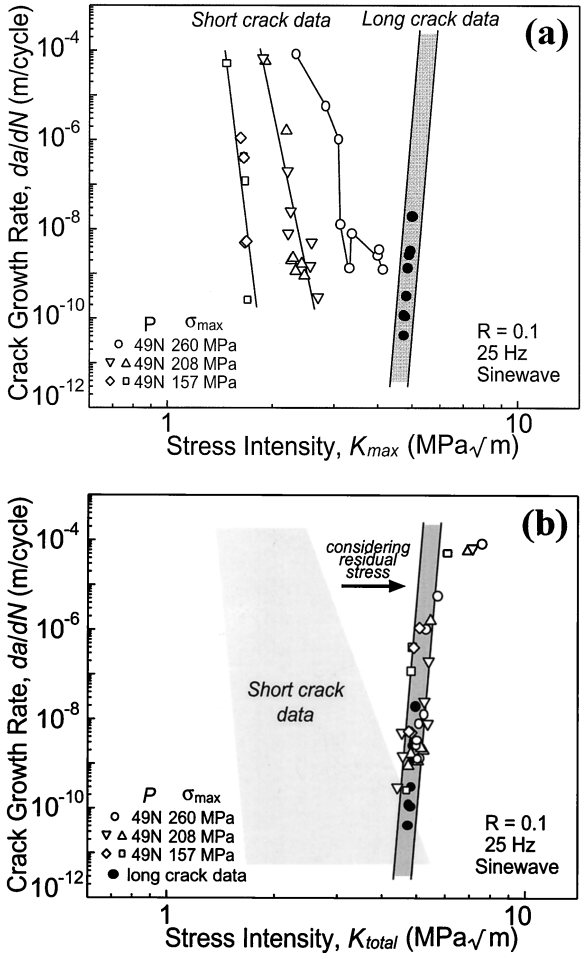

Fig. 6. (a) Small-crack growth data in 6A4Y-SiC from cantilever-beam specimens: (a) as a function of the applied K_{max}, compared with corresponding long-crack data derived from DC(T) specimens, (b) as a function of the total stress intensity ($K_{max} + K_{rd}$) where K_{rd} results from the residual stress surrounding the indent.

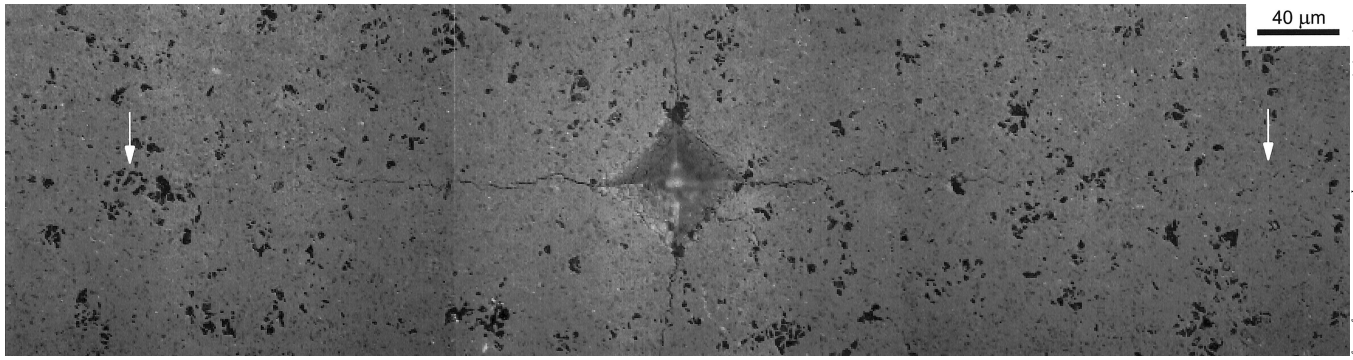

Fig. 7. An optical micrograph of the surface indent crack in 6A4Y-SiC after exposure to $\sim 1.4 \times 10^5$ cycles (white arrows indicate crack tips) at the stress of 260 MPa. Note the extensive crack growth normal to the applied cyclic stress.

Figure 3 shows the rising *R*-curve behavior of 6A4Y-SiC; the solid line represents the stress distribution when fracture takes place. The *R*-curve is obtained by connecting the common tangent line of stress function, and represented by a thick gray line. In the case of 6A4Y-SiC, the initiation toughness is ~4 MPa·m$^{1/2}$ and rises to a maximum value of 6.2 MPa·m$^{1/2}$, due to the development of a crack wake zone. In contrast, Hexoloy SA shows no such rising *R*-curve, consistent with its transgranular fracture mode and consequent lack of wake bridging.

(3) Long- and Small-Crack Growth Behavior

The variation in fatigue-crack growth rates, as a function of the applied stress intensity, is shown for long (>3 mm) cracks in 6A4Y-SiC in Fig. 4. These results show a marked dependency of growth rates on the value of the applied stress intensity. The effect of load ratio can be seen by comparing Figs. 4(a) and (b), where growth rates are respectively plotted as a function of ΔK and K_{max}. At a fixed ΔK, growth rates are accelerated, and the threshold ΔK_{th} reduced, with increasing *R* (Fig. 4(a)). However, at a fixed K_{max} growth rates are slightly decreased with increasing *R* (Fig. 4(b)), indicative of the small ΔK dependence.

Crack length versus number of cycles data used in determining the corresponding growth rates of the small (>200 μm) surface cracks, at various stress levels, is shown in Fig. 5, based on observations of the tensile surface of the cantilever beams. Of note is the fact that the growth rates of the small cracks tend generally to decrease as their size is increasing. Using linear-elastic solutions, such data are plotted to growth rate as a function of K_{max} and the total stress intensity, incorporating the residual stresses induced by the indentation, K_{total} ($=K_{max} + K_{rd}$), respectively. Similar behavior has been reported in Mg-PSZ, ABC-SiC, and Al_2O_3–SiC_w.[12,13,20] In general, the small-crack effect results from the competition of the driving force for crack propagation based on the applied stresses (which increase with increasing crack length), and the specific toughening mechanism which inhibits crack propagation (which also increases with crack length until an equilibrium bridging zone is formed). In the present study, there is no significant difference between small- and long-crack data if the residual stresses, K_{rd}, from the indent are considered (in Fig. 6(b)). This means that steady-state shielding is probably achieved during the rapid growth of cracks in the first few loading cycles. An image of a crack that has grown to nearly 300 μm is shown in Fig. 7. The scatter in the small-crack data in Fig. 6(a) also reflects how the small crack shows a greater sensitivity to local microstructural inhomogeneities. As seen in whisker-reinforced composites and *in situ* toughened ceramics such as Al_2O_3–SiC_w and ABC–SiC,[7,20] such scatter has been considered to be associated with the interaction of crack tips with local microstructure obstacles of dimensions comparable with crack sizes.

IV. Conclusions

Based on a study of *R*-curve behavior and crack propagation behavior of both long- (through-thickness) and small- (indent-initiated) cracks in a liquid-phase-sintered SiC under cyclic loads, the following conclusions can be drawn:

(1) Rising *R*-curve behavior is shown ranging from 4 to 6.2 MPa·m$^{1/2}$ and due to a crack bridging mechanism via platelike grains.

(2) The measurements establish that flaws greater than ~200 μm in size behave like long through-thickness cracks under cyclic loads after accounting for indent-induced residual stresses.

References

[1]D. H. Kim and C. H. Kim, "Toughening Behavior of Silicon Carbide with Additions of Yttria and Alumina," *J. Am. Ceram. Soc.*, **73** [5] 1431–34 (1990).

[2]N. P. Padture, "*In Situ* Toughened Silicon Carbide," *J. Am. Ceram. Soc.*, **77** [2] 519–23 (1994).

[3]S. K. Lee and C. H. Kim, "Effects of α-SiC versus β-SiC Starting Powders on Microstructure and Fracture Toughness of SiC Sintered with Al_2O_3–Y_2O_3 Additives," *J. Am. Ceram. Soc.*, **77** [6] 1655–58 (1994).

[4]S. K. Lee, D. K. Kim, and C. H. Kim, "Flaw-Tolerance and *R*-curve Behavior of Liquid-Phase-Sintered Silicon Carbide with Different Microstructures," *J. Am. Ceram. Soc.*, **78** [1] 65–70 (1995).

[5]M. A. Mulla and V. D. Krstic, "Mechanical Properties of β-SiC Presureless Sintered with Al_2O_3 Additions," *Acta Metall. Mater.*, **42** [1] 303–308 (1994).

[6]Y. W. Kim, M. Mitomo, and H. Hirotsuru, "Grain Growth and Fracture Toughness of Fine-Grained Silicon Carbide Ceramics," *J. Am. Ceram. Soc.*, **78** [11] 3145–48 (1995).

[7]J. J. Cao, W. J. MoberlyCahn, L. C. DeJonghe, C. J. Gilbert, and R. O. Ritchie, "*In Situ* Toughened Silicon Carbide with Al-B-C Additions," *J. Am. Ceram. Soc.*, **79** [2] 461–69 (1996).

[8]R. F. Cook, C. J. Fairbanks, B. R. Lawn, and Y.-W. Mai, "Crack Resistance by Interfacial Bridging: Its Role in Determining Strength Chacteristics," *J. Mater. Res.*, **2** [3] 345–56 (1987).

[9]P. L. Swanson, C. J. Fairbanks, B. R. Lawn, Y.-W. Mai, and B. J. Hockey, "Crack-Interface Grain Bridging as a Fracture Resistance Mechanism in Ceramics: I, Experimental Study on Alumina," *J. Am. Ceram. Soc.*, **70** [4] 279–89 (1987).

[10]S. J. Bennison and B. R. Lawn, "Role of Interfacial Grain-Bridging Sliding Friction in the Crack-Resistance and Strength Properties of Non-Transforming Ceramics," *Acta Metall.*, **37** [10] 2659–71 (1989).

[11]C. J. Gilbert, J. J. Cao, W. J. Moberlychan, L. C. DeJonghe, and R. O. Ritchie, "Cyclic Fatigue and Resistance-Curve Behavior of an *In Situ* Toughened Silicon Carbide with Al-B-C Additions," *Acta Metall. Mater.*, **44** [8] 3199–214 (1996).

[12]A. A. Steffen, R. H. Dauskardt, and R. O. Ritchie, "Cyclic Fatigue Life and Crack-Growth Behavior of Microstructurally Small Cracks in Magnesia-Partially-Stabilized Zirconia Ceramics," *J. Am. Ceram. Soc.*, **74** [6] 1259–68 (1991).

[13]C. J. Gilbert, J. J. Cao, L. C. DeJonghe, and R. O. Ritchie, "Crack-Growth Resistance-Curve Behavior in Silicon Carbide: Small versus Long Cracks," *J. Am. Ceram. Soc.*, **80** [9] 2253–61 (1997).

[14]Y. S. Han, D. K. Kim, C. J. Gilbert, and R. O. Ritchie, "Effect of Stacking Fault on the Grain Shape in Liquid-Phase-Sintered Silicon Carbide," unpublished work.

[15]L. M. Braun, S. J. Bennison, and B. R. Lawn, "Objective Evaluation of Short-Crack Toughness Curve Using Indentation Flaws: Case Study on Alumina-Based Ceramics," *J. Am. Ceram. Soc.*, **75** [11] 3049–57 (1992).

[16]J. C. Neuman and I. S. Raju, "Stress-Intensity Factor Equations for Cracks in Three-Dimensional Finite Bodies Subjected to Tension and Bending Loads," NASA Technical Memorandum 85793, NASA Langley Research Center, Hampton, VA, April 1984.

[17]D. R. Clarke, "On the Equilibrium Thickness of Intergranular Glass Phases in Ceramic Materials," *J. Am. Ceram. Soc.*, **70** [1] 15–22 (1987).

[18]I. Tanaka, H. J. Kleebe, M. K. Cinibulk, J. Bruley, D. R. Clarke, and M. Ruhle, "Calcium-Concentration Dependence of the Intergranular Film Thickness in Silicon Nitride," *J. Am. Ceram. Soc.*, **77** [4] 911–14 (1994).

[19]G. Pezzotti, H. J. Kleebe, and K. Ota, "Grain-Boundary Viscosity of Polycrystalline Silicon Carbides," *J. Am. Ceram. Soc.*, **81** [12] 3293–99 (1998).

[20]R. H. Dauskardt, M. R. James, J. R. Porter, and R. O. Ritchie, "Cyclic Fatigue-Crack Growth in a SiC-Whisker-Reinforced Alumina Ceramic Composite: Long- and Small-Crack Behavior," *J. Am. Ceram. Soc.*, **75** [4] 759–71 (1992). □